Response of OH airglow emissions to the mesospheric gravity waves and its comparisons with full wave model simulation at a low latitude Indian station

R. N. Ghodpage[1], M. P. Hickey[2], A. Taori[3,4], Devendraa Siingh[5] and P. T. Patil[1]

[1] {Indian Institute of Geomagnetism, Shivaji University Campus, Kolhapur 416004, India}

[2] {Embry-Riddle Aeronautical University, FL - 32114, USA}

[3] {National Atmospheric Research Laboratory, Pakala Mandal, Gadanki (A. P.) 517112, India}

[4] {now at- National Remote Sensing Center (NRSC), Hyderabad, 500037, India}

[5] {Indian Institute of Tropical Meteorology, Pune-411 008, Maharashtra, India}

Abstract:

The quasi-monochromatic gravity wave induced oscillations, monitored using the mesospheric OH airglow emission over Kolhapur (16.8°N and 74.2°E), India during January to April 2010 and January to December 2011, have been characterized using the Krassovsky method. The nocturnal variability reveals prominent wave signatures with periods ranging from 5.2-10.8 hr as the dominant nocturnal wave with embedded short period waves having wave periods 1.5-4.4 hr. The results show that the magnitude of the Krassovsky parameter, viz., |η| ranged from 2.1 to 10.2 for principal or long nocturnal waves (5.2 to10.8 hr observed periods), and, from 1.5 to 5.4 for the short waves (1.5 to 4.4 hr observed periods) during the years of 2010 and 2011, respectively. The phase, i.e., Φ values of the Krassovsky parameters exhibited larger variability and varied from −8.1° to −167°. The deduced mean vertical wavelengths are found to be approximately −60.2 ± 20 km and – 42.8 ± 35 km for long and short wave periods for the year 2010. Similarly, for 2011 the mean vertical wavelengths are found to be approximately −77.6 ± 30 km and – 59.2 ± 30 km for long and short wave periods, respectively, indicating that the observations over Kolhapur were dominated by upward propagating waves. We use a full wave model to simulate the response of OH emission to the wave motion and compare the results with observed values. In the present report, we discuss the observed wave characteristics and cause of the noted differences.

Keywords: OH emissions, Mesospheric gravity wave, Full wave model

1. Introduction

Often the observed temporal variations in the mesospheric hydroxyl OH night airglow intensities and rotational temperatures are caused by the propagating gravity waves from the lower to the upper atmosphere. The interaction of these upward propagating waves with the ambient and other waves contribute to the dynamical variability, which in turn is reflected in observed airglow intensity and temperature perturbations (Hines, 1997). Krassovsky (1972) introduced a quantity 'η' to characterize the wave-induced perturbations. This parameter, termed as 'Krassovsky's parameter', can be defined as $\eta = |\eta| e^{-i\Phi}$, where $|\eta|$ indicates the ratio of the amplitude variation between the emission intensity and temperature perturbations normalized to their time averages and Φ is a phase difference between the intensity wave and its temperature counterpart (e.g., Walterscheid et al., 1987; Taylor et al., 1991). It should also be mentioned here that apart from the pure dynamical processes η can also be affected by various other unknown parameters, such as the variation of local oxygen photochemistry (Hickey et al., 1993) and height variation of the emission layer which affects emission rates and temperature directly (Liu and Swenson 2003; Vargas et al., 2007). Although this can complicate studies of Krassovsky's parameter, it offers an opportunity to study the above aspects at the same time. Overall, once the physics and chemistry of emissions are well understood, the η values would offer a good tool to study the perturbations caused in a parameter (temperature, brightness/intensity) by measuring one under adiabatic conditions.

Utilizing the above, many investigators have carried out observational as well as the theoretical studies on the identification and characterization of gravity wave and tidal signatures with wave periodicities ranging from few minutes to several hours (e.g., Walterscheid et al., 1987; Hecht et al., 1987; Hickey 1988a, b; Taylor et al., 1991; Takahashi et al., 1992; Reisin

and Scheer 1996; Taori and Taylor 2006; Guharay et al., 2008; Ghodpage et al., 2012, 2013). However, observational studies of the magnitude and phase of η over a range of wave periods for a given location and season are sparse. Some of the notable observations of η for the OH emission have been performed by Viereck and Deehr (1989) in the wave period range of ~ 1 - 20 hr and by Reisin and Scheer (1996) near to the semidiurnal tidal fluctuations.

In the present work, we utilize the mesospheric OH emission intensity and temperature data obtained during January - April 2010 and January - December 2011, when clear and moonless nights allowed observations to exceed 5 hours duration. We deduce the Krassovsky parameters as a function of observed wave period and also infer the vertical wavelengths for the observed mesospheric waves. Further, we compare our estimates with the earlier results reported by various investigators. We also employ a full-wave model to simulate the effects of wave motions on the OH airglow. This model has been used previously to compare observations and theory of airglow fluctuations (e.g., Hickey et al., 1998; Hickey and Yu 2005). Here, the model is used to estimate the values of the amplitudes and phases of Krassovsky's ratio which are compared to those derived from the observations, making the present study unique and the first of its kind over Indian latitudes.

2. Instrumentation and Observations

The mesospheric OH observations used in the present study are made using the multispectral photometer from Kolhapur (16.8°N, 74.2°E) (Ghodpage et al., 2013, 2014). We use the period of January - April 2010 and January- December 2011 when the availability of clear sky conditions prevailed for several nights. In particular, for 2010 data, out of 45 nights of OH airglow

78 measurements,14 nights clearly showed wavelike features, while in the 2011 year data, 60 nights
79 out of 30 nights exhibited wavelike variations.
80
81 **2.1 The multispectral photometer**
82 The multi-spectral photometer monitors airglow emissions at 731 and 740 nm rotational lines of
83 OH (8,3), O(^{1}S) 557.7 nm and O (^{1}D) 630.0 nm emissions near simultaneously. The low
84 temperature coefficient interference filters (10 cm aperture) used in the photometer have full
85 width at half maximum ~ 1 nm (transmission ~ 40–70% at 24°C). We kept the integration time
86 for each filter 10 seconds which results in repetition time of 90 seconds. The photometer has F/2
87 optics with full field of view ~10°. The stepper motor rotation and sensing of the initial position
88 is performed by computer controlled software. As the detector, the EMI9658B photomultiplier
89 tube is used. An amplifier (high gain trans-impedance) is used to to convert and amplify
90 photomultiplier's very weak (in the range of nA) output current in to corresponding voltage
91 form. This output is recorded in digital format in term of arbitrary units along with time which is
92 used for further processing.
93
94 **2.2 Full-Wave Model**
95 The full-wave model is a linear, steady-state model that solves the linearized Navier-Stokes
96 equations on a high resolution vertical grid to describe the vertical propagation of acoustic-
97 gravity waves in a windy background atmosphere including molecular viscosity and thermal
98 conduction, ion drag, Coriolis force and the eddy diffusion of heat and momentum in the
99 mesosphere. The model description, including equations, boundary conditions and method of
100 solution has been described elsewhere (Hickey et al., 1997; Walterscheid and Hickey 2001;

101 Schubert et al., 2003). The neutral perturbations are used as input to a linear, steady-state model
102 describing OH airglow fluctuations (Hickey and Yu 2005).

103 The model solves the equations on a high resolution vertical grid subject to boundary
104 conditions, and allows quite generally for the propagation in a height varying atmosphere (non-
105 isothermal mean state temperature and height varying mean winds and diffusion). The linearized
106 equations are numerically integrated from the lower to the upper boundary using the tri-diagonal
107 algorithm described by Bruce et al. (1958) and Lindzen and Kuo (1969). The lower boundary is
108 set well below the region of interest and a sponge layer is implemented to avoid effects of wave
109 reflection in the airglow response. In this study the lower boundary (the bottom of the lower
110 sponge layer) is placed at 250 km below z = 0 (i.e., -250 km). The wave forcing is through the
111 addition of heat in the energy equation. The heating is defined by a Gaussian profile with a full-
112 width-at-half-max of 0.125 km. It is centered at an altitude of 10 km. A Rayleigh-Newtonian
113 sponge layer in addition to natural absorption by viscosity and heat conduction prevents spurious
114 reflection from the upper boundary. At the upper boundary (here 300 km altitude) a radiation
115 condition is imposed using a dispersion equation that includes viscous and thermal dissipation
116 (Hickey and Cole 1987). The mean state is defined using the Mass Spectrometer Incoherent
117 Scatter (MSIS) model (Hedin 1991).

118 A set of linear perturbation equations for the minor species involved in the OH emission
119 chemistry is solved using the approach described in Hickey (1988). This assumes that these
120 minor species have the same velocity and temperature perturbations as the major gas (which are
121 deduced from the full-wave model). A vertical integration of the volume emission rates through
122 the vertical extent of the OH layer provides the brightness and brightness-weighted temperature
123 perturbations, from which Krassovsky's ratio is determined. The OH chemistry we use is the

same as that used previously (Hickey et al., 1997) and is for the OH (8-3) emission. We also determine the vertical wavelength at the peak of the OH emission layer evaluated from the phase variations of the temperature perturbations determined by the full-wave model.

2.3 Space borne measurements

The sounding of the atmosphere using broadband emission radiometry (SABER), on-board the thermosphere ionosphere mesosphere energetic and dynamics (TIMED) satellite, is a high-precision broadband radiometer which measures limb radiance (at 74°) of the terrestrial at in 10 selected spectral bands ranging from 1.27 to 15 μm. In the present study, we note larger values of $|\eta|$ occur during 2011 compared to 2010 for long/principal waves, which indicates a larger intensity to temperature perturbation ratio over Kolhapur during the passage of the waves during 2011. This could be due to the differences in either the background atmosphere or the dynamical processes of 2010 and 2011 years. To identify this, we scrutinize the OH volume emission rate profile for Kolhapur region (obtained from the SABER instrument on-board the thermosphere ionosphere mesosphere energetic and dynamics (TIMED) satellite. The selected latitude–longitude grids are 10°N to 20°N and 70°E to 90°E representing Kolhapur. The criteria for the selection of SABER data are such that: (i) the SABER pass should be during typical observation times (i.e. nighttime); (ii) it should not be at twilight.

3. Results and Discussion

To identify the wave structures in the data, we utilize the perturbation amplitudes normalized to their time averaged values (hereafter referred to as mean values) in the intensity and temperature data to calculate the Krassovsky ratio. To illustrate this, we show a typical example corresponding to the data obtained on 26-27 January 2011 in Figure 1. We plot the temperature

deviations (circles with connecting lines) from their mean values in figure 1(a), while, the intensity deviations (circles with connecting lines) from their mean values are plotted in figure 1(b). We note that night airglow intensity variations show a long-period wave with embedded short-period oscillatory features. On this night, the mean of airglow intensity is found to be ~ 1.83 arbitrary units and the mean of the temperature data is ~ 195.75 K. To identify the nocturnal variability plotted together with data are the results (shown as red solid lines) of best-fit cosine model (e.g., Taori et al., 2005) as follows.

$$Y = A\cos\left[\pi\frac{(X - Xc)}{T}\right] \quad (1)$$

where, A is the amplitude of the fitted wave of half-period T with phase Xc , and X is the time. Note that the solid red lines in figure 1 show the results of the best-fit cosine model. We observed the presence of ~ 8.2 ± 1.1 hr and 8 ± 1.3 hr waves with relative amplitudes ~ 7.57 and 54.5%, in the nocturnal temperature and intensity variability, respectively. Given the uncertainties involved in the observations, we consider these to be the same waves. Further, we compute the |η| value for this wave to be 7.2 ± 1.3. To identify the shorter period features in the data we obtain residuals from the best-fit model values (Figure 1c). The bottom-left (Figure 1c) and bottom-right (Figure 1d) panels show the nocturnal variability of the residual temperature and intensity, respectively. The best-fit model reveals the presence of ~ 4.0 ± 0.2 and 3.0 ± 0.8 hr wave in the temperature and intensity residuals, respectively. Once again we treat these as the same wave for the reason explained above. The best-fit analysis shows the percentage amplitudes of this wave to be ~ 4.1 K and 15.1 arbitrary units in the temperature and intensity data, respectively. Hence, the |η| value for short period waves is estimated to be 3.7 ±0.9. The phase difference between the intensity and temperature waves is obtained with the help of best-fit

168 parameters which were also verified with a cross correlation analysis. The phase of the principal
169 waves (maxima) (period ~8.2 hr) was ~ 25.02 hr in the temperature data and 24.6 hr in the
170 intensity data, which results in the phase difference of ~ 0.4 hr, i.e., Φ values of −18.0±10°.
171 Similarly, for the shorter period (period ~ 4 hr) the Φ values are estimated to be −100.8±22°.
172 We can also estimate the vertical wavelength with the help of Krassovsky's parameter following
173 the approach of Hines [1997]:

174 $$\lambda z = \frac{2\pi\gamma H}{(\gamma - 1)|\eta| \sin(\phi)} \quad (2)$$

175 where $\gamma = C_p / C_v = 1.4$ is the ratio of specific heats, and H = 6 km is the scale height. This
176 formula is valid for zenith observations and for plane waves. It is not valid for the evanescent
177 waves. Using the above relation we find that vertical wavelength for the two cases discussed
178 above are ~ −39± 15 and −35.5± 10 km for long period and short period waves, respectively. Note
179 that the long period wave estimates may be biased when the data length is comparable to that of
180 the wave period and therefore in our study we have considered only those waves whose periods
181 are substantially less than the length of the available data.

182 The above analysis was carried out on nighttime events recorded during 2010 and 2011
183 when the prominent wave features were visible. One may note that during the 2010 period, the
184 principal nocturnal waves in the data show the wave periods vary from 5.2 to 10.8 hr with
185 corresponding temperature amplitudes ranging from 0.2 to 13.8 K. Similarly for 2011, wave
186 periods vary between 5.2 and 8.4 hr with corresponding temperature amplitudes lying between
187 0.7 K and 15.7 K. However, the intensity amplitudes of the principal waves vary from 1.5% to
188 56.5% and 5% to 90% for 2010 and 2011, respectively. We note that the estimated |η| values
189 were found to range from 2.1 - 10.5 for the principal wave. In the case of the short period waves,

190 the periods varied from 1.5 to 4.4 hr (for 2010) and 2.8 to 4.4 hr (for 2011) with corresponding
191 temperature amplitudes ranging from 0.2 K to 12.5 K and 0.4 K to 14.4 K. The corresponding
192 intensity amplitudes varied from ~ 1.8% to 56% and 0.8% to 46.8% for 2010 and 2011,
193 respectively. The phase (Φ) values also exhibit large variability for long (short) period waves,
194 varying between −27° and −167° (−27° and − 150°) for 2010 and -8.1° and -65.2° (-39.1° and -
195 122.6°) for 2011. For 2010 the deduced vertical wavelengths are found to vary from – 32.2 km
196 to −140 km and −24 km to −88 km for the long and short period waves, respectively. Similarly,
197 for 2011 the deduced vertical wavelengths are found to vary from − 40 km to −102 km, and −26
198 km to −92.4 km for the long and short period waves, respectively.

199 In Figure 2a we plot our results for |η| (hereafter η) with pink half-filled squares
200 indicating the estimates for the year 2010 and olive half-filled squares for the year 2011. We plot
201 Φ in Figure 2b using the same symbols as used in Figure 2a. For a comparison, we also show the
202 values of η and Φ reported by other investigators (Viereck and Deehr 1989; Takahashi et al.,
203 1992; Oznovich et al., 1995, 1997; Drob 1996; Reisin and Scheer 1996; Taylor et al., 2001;
204 Lopez-Gonzalez et al., 2005). Also shown in the figure are the model estimates of Schubert et al.
205 (1991), Tarasick and Shepherd (1992a, b), Walterscheid and Schubert (1995). In general, we
206 observe that the parameter η increases with wave period. It is evident that the observed η and Φ
207 values in our study show a large spread in their distribution as compared to the model values. A
208 similar spread in the distribution of observed values of η (Figure 2a) from 1.03 to 7.85 has also
209 been observed by other investigators (e.g., Takahashi et al., 1992). It may be noted that the
210 values of η for the OH data in our study lie somewhere between the model estimates and the
211 values observed by other investigators. Also noteworthy in this figure is that our η values are
212 closer to the model values reported by Tarasick and Shepherd (1992a) for the waves with

horizontal wavelength 500 km. The phase 'Φ' values, on the other hand show significantly larger deviations from this model for 2010, while for 2011 the match between measured and modeled phases appear to be better. We note that our measurements of Φ matches somewhat with those reported by Viereck and Deehr (1989), while large differences with other investigators can be easily noted. The variation of Φ values with respect to the wave periodicity, obtained in the 2010 year clearly shows that most of the time we observe values to be higher than those obtained by different models.

In particular, Reisin and Scheer (1996) found mean (arithmetic) value of η to be 5.5 ± 0.6 and the mean Φ value to be − 66° for OH. Our observed values of η (arithmetic mean, 4.4± 1 for 2010 year and 5.7±1.7 for 2011 year) near by agree with the values reported by Reisin and Scheer (1996) for OH measurements. In a further report, based on 5- year observations, Reisin and Scheer (2004), found the mean value of η to be ~5.6 for the nightly semidiurnal type waves and ~3.4 for the waves of 3000 s periodicity; which is in agreement with our values. In another study based on long-term observations with a spectral airglow temperature imager (SATI) from a mid-latitude station, Lopez-Gonzalez et al. (2005) reported a mean value of η of approximately ~ 8.6 for the OH measurements with a larger variability than our observations show. In another report, Guharay et al. (2008), found that for wave periods ranging from 6 hr to 13 hr, values of η varied from 1.7 to 5.4, while the phase varied from −13^{o} to − 90°. Similarly, Aushev et al. (2008) presented amplitudes of the Krassovsky parameter for wave periods of 2.2 to 4.7 hr which varied from 2.4 to 3.6 while the phase varied from – 63^{o} to −121°. It is noteworthy that our derived values broadly agree with Guharay et al. (2008, 2009), Reisin and Scheer (1996, 2004) and Viereck and Deehr (1989) while they are somewhat different from the values reported by

235 Lopez-Gonzalez et al. (2005) (which may be due to the fact that their observations corresponded
236 to higher latitude than ours).

237 In general, the results shown in Figure 2 emphasize that there are significant in the
238 Krassovsky parameters derived from one study to another. This we suspect to be caused by the
239 variations in the altitudinal profile of oxygen and its effect on the η through the complex OH
240 chemistry (Walterscheid et al., 1994). Another possibility over low latitudes was discussed by
241 Makhlouf et al. (1995) who suggested the quenching caused by the perturbed molecules during
242 their transitions from several vibrational levels. Winds also affect the OH response to gravity
243 waves and therefore they will also contribute to the spread of values seen between the various
244 observation studies.

245 Note that our observations as well as models show the phase Φ for OH to be a negative
246 value indicating the upward propagating waves. In general we note that our Φ values, although
247 on some occasions are closer to Viereck and Deehr (1989) observations, show large deviations
248 from other investigators and are larger than the model values on most occasions. Differences in
249 theory and observation may be due to the horizontal wavelength assumed in the model and or the
250 Prandtl number (ratio of kinematic viscosity to thermal diffusivity) assumed. The Prandtl number
251 is important in theoretical calculations and modeling, especially when in terms of dissipating
252 waves owing to molecular viscosity and thermal diffusivity while they propagate in the
253 atmosphere (Hickey 1988). An error in the Prandtl number assumption will affect the derived
254 wave parameters (λ_z, η etc.), which will successively mask the actual ones. In this regard,
255 Makhlouf et al. (1995) studied the variations in the η values by modifying the model proposed by
256 Hines and using a photochemical dynamical model; however, they were still unable to explain
257 the appearance of the negative phases appropriately. Hines and Tarasick (1987) found a wide

range of η variability, a result supported by our measurements. Further, Hines and Tarasick (1997) subsequently discussed the necessary correction for thin and thick layer approximations for the calculation of η from airglow emissions due to gravity waves interaction. They also pointed out that OH emission intensity, which affects the derived η values, does not depend on the oxygen profile and other minor species, which contradicts the theory of Walterscheid et al. (1994), Schubert et al. (1991) and Offermann et al. (1981).

The calculated vertical wavelengths (VW) for all the nights of the observation are shown in Figure 2c as pink half filled squares indicating the estimates for the year 2010 and olive half filled squares for the year 2011. Large differences exist from one night to another. The VW has a large variability varying from – 41 km to −102 km (2010) and – 36.2 km to −140 km (2011) for long period waves, and, – 26 to −92.4 and – 24 to −88 km for short period waves period of 2010 and 2011 years respectively. In 2010 (and 2011) years, the mean VW values for long and short period waves are calculated to be −60.2 ± 20 km (−77.2 ± 40 km) and –42.8 ± 15 km (–59.2 ± 30) respectively. All the observations show negative values for Φ and λ_z, indicating upward propagating waves. Further, unlike the clear dependency on the wave period noted in the Krassovaky parameters (η and Φ) no clear trend is noted in the calculated VW. We also plot the values reported by Reisin and Scheer (1996) and Lopez-Gonzalez et al. (2005) for a comparison. It is noteworthy that for all the days the VW for the long period wave are higher than the VW of short period waves. We also observed that VW values calculated for 2011 year are larger than 2010 year calculated values.We note that the values reported by Reisin and Scheer (1996) are approximately −30 km with about 40 km variability, which is a good agreement with our values. However, Lopez-Gonzalez et al. (2005) observed VW values to be approximately −10 km deduced from their OH observations, which do not agree with our values. Further, Ghodpage et

281 al. (2012) analyzed the long-term nocturnal data of 2004-2007 and also observed that the VW
282 lies between 28.6 and 163 km. Recently, Ghodpage et al. (2013) studied the simultaneous
283 mesospheric gravity wave measurements in the OH emission from Gadanki and Kolhapur,
284 inferring mean VWs varying from – 26 to – 60 km for the Kolhapur observations. Takahashi et
285 al. (2011) reported vertical wavelengths varying from 20 to 80 km, which is in agreement with
286 our values.
287
288 **4. Comparison with the full wave model Results**
289 Wave simulations were performed using the full-wave model **(FWM)**. The observations
290 were conducted over an approximate one month period spanning February 8th and March 13th,
291 and accordingly we used the middle date of this observation period (February 25th) in the MSIS
292 model to represent the undisturbed mean state. The latitude used was 16.8° N, and the local time
293 was midnight. Because the speed and direction of wave propagation were not determined from
294 the observations, several simulations were performed for each wave period in which the direction
295 of propagation (eastward, northward and westward propagation) and the phase speed (50 m/s,
296 100 m/s and 150 m/s) were varied. Note that the mean winds (not shown) in these simulations
297 were derived from the Horizontal Wind Model (HWM) using the same input parameters as used
298 for the MSIS model. The derived meridional winds (not shown) are far smaller than the zonal
299 winds for the conditions considered here, and so while results for eastward and westward
300 propagation differed quite markedly, those for northward and southward propagation did not.
301 Hence we considered only a single direction (northward) for meridional propagation.
302 We also performed a tidal simulation using an equivalent gravity wave model (Lindzen
303 1970; Richmond 1975), as implemented in an earlier study (Walterscheid and Hickey 2001).

304 The horizontal wavelength and Coriolis parameter are adjusted to give maximal correspondence
305 with a given tidal mode. Here, we performed calculations for the terdiurnal (3,3), (3,4), (3,5) and
306 (3,6) modes using parameters provided by Richmond (1975). The simplifications inherent in this
307 approach are discussed by Walterscheid and Hickey (2001).

308 Comparisons between the full wave model results for η, Φ and λ_z and the values inferred
309 from the observations are shown in figure 3a, 3b and 3c, respectively. In figure 3a we compare
310 the observed values of η for 2010 and 2011. show The observed values of η are represented as
311 pink and olive lower half-filled squares for 2010 and 2011, respectively. In figure 3a we note that
312 at few of the longer wave periods, the observed values of η are in good agreement with the full
313 wave model results. For short period waves the values of η inferred from the observations appear
314 to be bounded by the model values for waves with horizontal phase velocities are 50 - 100 m/s,
315 respectively. For example, for 3.6 hr wave periods, the average of the values of η inferred from
316 the observations is 3.7, while the full wave model values lie between about 0.5 (for the 100 m/s
317 wave) and 7 (for the 50 m/s, eastward propagating wave). For the 8 hr wave periods, the average
318 of the values of η inferred from the observations is 5.7, which is bounded by the full wave model
319 estimates for waves having a horizontal phase velocity of 50 m/s and different propagation
320 directions.

321 Overall, we note that that the comparison between the observed η values and the modeled
322 values can be explained by gravity waves whose horizontal phase velocities range from 50 m/s to
323 100 m/s. In this regard, an earlier investigation by Pragati Sikha et al. (2010) reported observed
324 gravity wave horizontal phase speeds (for periods 5 min to 17 min) varying between 10 m/s and
325 48 m/s. The propagation directions were reported to be preferentially towards the north. More
326 recently, Taori et al. (2013) studied mesospheric gravity wave activity in the OH and OI 558 nm

emissions from Gadanki. They observed that the gravity waves were moving in the north–west direction. The average phase velocity of the ripple-type waves was found to be 23.5 m/s. The other, band-type waves, with horizontal scales of about 40 km, were found to be propagating from south to north with an estimated phase speed of 90 m/s.

The vertical wavelengths (λ_z) calculated using the observed values of η and Φ differ significantly from the full wave model estimate for waves with phase velocities below 100 m/s. More typically, a comparison between those values inferred from the observations and those derived from the model tend to agree for phase velocities in the 100 – 150 m/s range. However, it should be noted that vertical wavelengths inferred from the observations are based on the use of the inferred Krassovsky's ratio, η, in Eq. (2). Errors in the determination of the phase (Φ) of η can lead to significant errors (proportional to $\cot\Phi$) in the determination of λ_z, especially as Φ approaches $\pm 180^o$.

The differences noted in the observed and modeled estimates of Krassovsky ratio magnitudes η and phase (Φ) may be associated with the limitation arising due to dynamics as well as the measurements. In terms of measurements limitation, the parameters achieved with the best fit method may have leaked contribution from other wave components which may be dynamically varying within a wave period. In terms of dynamics, that full wave model uses climatological density (both major gas and minor airglow-related species) and wind profiles which will introduce uncertainties. This point has been previously elaborated by Walterscheid et al. (1994) with respect to the effect of a change in the [O] profile on the OH response to wave motions.

The differences noted in the magnitude of the observed Krassovsky ratio η between 2010 and 2011 may be associated with variations in the height and shape of the undisturbed OH

emission profile. To check whether there was a difference in the OH emission layer structure, we selected the nighttime OH emission profile for a grid encompassing 10^{o}N to 20^{o}N latitudes and 70^{o}E to 90^{o}E latitudes during February, March and April months of the years 2010 and 2011. We have selected the February to March period because the optical airglow data used in this study was acquired primarily during these months. The monthly mean values of OH emission rates are plotted in **Figure 4**. The solid curves correspond to 2010 data while the dashed curves correspond to 2011 data for . We note that the peaks of OH emission layer during February, March and April of 2010 occurred at 84.2 km, 82.8 km and 85.1 km altitude, respectively, while the corresponding peaks for 2011 were found to occur at 85.8 km, 85.6 km and 85.2 km altitude. This suggests that the peak of the emission layer occurred at a somewhat lower altitude in 2010 compared to 2011. Also, the mission rates during February and March were found to be higher in 2010. It is important to note that in an earlier study, Ghodpage et al. (2013) compared the Krassovsky ratios at two different latitudes, Gadanki (13.5 N, 79.2E) and Kolhapur (16.8°N and 74.2°E) and noted a lower OH emission layer peak over Kolhapur and also larger estimated η values over Kolhapur. In the present case, instead of the location, it is the difference in the measurement year where the peak emission altitudes of the OH emission layer are somewhat diffterent. As the peak emission layer arise due to the chemical reactions involving odd oxygen, it is proposed that chemical constutents composition were different from the year 2010 to the year 2011. Therefore, the noted emission rates may be responsible for the observed differences in the Krassovsky parameters. A further question arise here is why the peaks should be different from one year to the other. As these months are pre-monsoon, when a large scale oscillation namely,El Niño/Southern Oscillation (ENSO) sweeps through the south Asian continent, we looked at the ENSO strength based on the Multivariate ENSO Index (MEI). This index is shown

373 in table 1, where it is noteworthy that the MEI index for 2010 (January to May) is of opposite
374 sign to that for the corresponding months in 2011. We postulate that these large scale processes
375 have a profound impact on the observed wave energetics and dynamics at mesospheric altitudes.
376 Large scale processes induced the wave oscillations associated with the ENSO. The ENSO generates a
377 spectrum of waves which are of planetary scales. These are expected to generate a secular variation in
378 temperature and density structure throughout the atmosphere. A difference in ENSO suggests that these
379 forcing are different in the two years (2010, 2011). At present, we do not know through which
380 process the ENSO may have implications in the observed wave characteristics. However, we
381 believe that further investigation is required in order to confirm whether or not any such
382 associations really do exist.
383
384 **5. Concluding remarks**
385 We report the Krassovsky parameters for the observed gravity waves from Kolhapur (16.8°N and
386 74.2°E) and their comparison with the full wave model. Following are the concluding remarks of
387 the present investigations.
388 1) It is evident that the observed values of Krassovsky parameters in our study show a large
389 spread in their distribution as compared to the model values (shown in Figure 2a). A
390 similar spread in the distribution has also been reported by other investigators. We have
391 also observed that more magnitude of η values in 2011 year than 2010 year.
392 2) It is also notable that the values of η for the OH data in our study lie between the model
393 estimates and the values observed by other investigators. Whereas the phase values are
394 more than the model values on most occasions. We note that our Φ measurements match

with those reported by Viereck and Deehr (1989), while they show large differences with other investigators values.

3) Observed vertical wavelength (VW) values broadly agree with the range reported by other investigators and are found to vary from −26 to −140 km.We also noted that VW values calculated for 2011 year are larger than 2010 year calculated values. Most of wave propagating upward in direction.

4) Comparison of observed η and Φ values agree fairly well with the full wave model results for waves with 50-100 m/s horizontal phase velocities. Vertical wavelengths tend to agree for waves with 100-150 m/s horizontal phase velocities, except for the longest period waves for which vertical wavelength cannot be reliably inferred from the observations.

The database used in the present study is limited in terms of the length and locations and based on the above conclusions, more rigorous study using coordinated observations and modeling are underway with an aim to uncover the physics occurring at upper mesosphere.

Acknowledgements

This work is carried out under the research grant funded by Ministry of Science and Technology and Department of Space, Govt. of India. RNG thank the Director, Indian Institute of Geomagnetism (IIG), Navi Mumbai for encouragement to carry out this work. The night airglow observations at Kolhapur were carried out under the scientific collaboration program (MoU) between IIG, Navi Mumbai and Shivaji University, Kolhapur. MPH acknowledges the support of NSF grant AGS-1001074.

418 **6. References**

419 Aushev, V. M., Lyahov, V. V., Lopez-Gonzalez, M. J., Shepherd, M. G., and Dryna, E. A. :Solar
420 eclipse of the 29 March 2006: results of the optical measurements by MORTI over Almaty
421 (43.03°N, 76.58°E), J. Atmos. Sol. Terr. Phys., 70, 1088–1101, 2008.

422 Bruce, G. H., Peaceman, D. W., Rachford, Jr. H. H., and Rice, J. D.: Calculations of unsteady-
423 state gas flow through porous media, Petrol. Trans. AIME, 198, 79-92, 1953.

424 Drob, D. P.: Ground-based optical detection of atmospheric waves in the upper mesosphere and
425 lower thermosphere, Ph. D. Thesis, University of Michigan, Ann Arbor, MI., 1996.

426 Ghodpage, R. N., Singh, D., Singh, R. P., Mukherjee, G. K., Vohat, P., and Singh, A. K.: Tidal
427 and gravity waves study from the airglow measurements at Kolhapur (India), J. Earth Syst.
428 Sci.121, 6, 1511–1525, 2012.

429 Ghodpage, R. N., Taori, A., Patil, P. T., and Gurubaran, S.: Simultaneous mesospheric gravity
430 wave measurements in OH night airglow emission from Gadanki and Kolhapur – Indian low
431 latitudes, Currents Science, 104, 1, 98-105, 2013.

432 Ghodpage, R.N., Taori, A., Patil, P. T., Gurubaran, S., Sharma, A. K., Nikte, S., and Nade, D.:
433 Airglow Measurements of Gravity Wave Propagation and Damping over Kolhapur (16.8^{o} N,
434 74.2^{o} E), International Journal of Geophysics (IJG), Volume 2014,1-9,
435 http://dx.doi.org/10.1155/2014/514937, 2014.

436 Guharay, A., Taori, A., Bhattacharjee, B., Pant, P., Pande, P., and Pandey, K.: First ground-
437 based mesospheric measurements from central Himalayas, Current Science, 97, 664-669,
438 2009.

439 Guharay, A., Taori, A., and Taylor, M.: Summer-time nocturnal wave characteristics in
440 mesospheric OH and O2airglow emissions, Earth Planets Space, 60, 973–979, 2008.

441 Hecht, J. H., et all.: Observations of wave-driven fluctuations of OH nightglow emission bfrom
442 Sondre Stromfjord, Greenland, J. Geophys. Res., 92, 6091-6099, 1987.

443 Hedin, A. E. :Extension of the MSIS thermosphere model into the middle and lower atmosphere,
444 J. Geophys. Res., 96, 1159 – 1172, 1991.

445 Hickey, M. P., and Yu, Y.: A full-wave investigation of the use of a "cancellation factor" in
446 gravity wave-OH airglow interaction studies, J. Geophys. Res., 110, A01301,
447 doi:10.1029/2003JA01372, 2005.

448 Hickey, M. P., Huang, T.Y., and Walterscheid, R. L.: Gravity wave packet effects on chemical
449 exothermic heating in the mesopause region, J. Geophys. Res., 108(A12), 1448,
450 doi:10.1029/2002JA009363, 2003.

451 Hickey, M. P., Walterscheid R. L., and Schubert, G.: Gravity wave heating and cooling in
452 Jupiter's thermosphere, Icarus, 145, 140-146, 2000.

453 Hickey, M. P., Walterscheid, R. L., Taylor, M. J., Ward, W., Schubert, G., Zhou, Q., Garcia, F.,
454 Kelley, M. C., and Shepherd G. G.: Numerical simulations of gravity waves imaged over
455 Arecibo during the 10-day January 1993 campaign, J. Geophys. Res., 102, 11,475-11,489,
456 1997.

457 Hickey, M.P., Schubert, G., and Walterscheid, R. L.: Gravity wave-driven fluctuations in the o_2
458 atmospheric (0-1) nightglow from an extended, dissipative emission region, J. Geophys.
459 Res., 98, 13,717-13,730, 1993.

460 Hickey, M. P.: Effects of Eddy Viscosity and Thermal Conduction and Coriolis Force in the
461 Dynamics of Gravity Wave- Driven Fluctuations in the OH Nightglow, J. Geophys. Res., 93,
462 4077, 1988.

463 Hickey, M. P., and Cole, K. D.: A quartic dispersion equation for internal gravity waves in the
464 thermosphere, J. Atmos. Terr. Phys., 49, 889-899, 1987.

465 Hines, C. O.: A fundamental theorem of airglow fluctuations induced by gravity waves, J.
466 Atmos. Sol. Terr. Phys.,59, 319–326, 1997.

467 Hines, C. O., and Tarasick, D. W.: Layer truncation and the Eulerian/ Lagrangian duality in the
468 theory of airglow fluctuations induced by gravity waves, J. Atmos. Sol. Terr. Phys., 59, 327–
469 334, 1997.

470 Hines, C. O., and Tarasick, D. W. : On the detection and utilization of gravity waves in airglow
471 studies, Planet Space Sci., 35, 851–866, 1987.

472 Krassovsky, V. I.: Infrasonic variation of OH emission in the upper atmosphere, Ann. Geophys.,
473 28, 739–746, 1972.

474 Lindzen, R. S.: Internal gravity waves in atmospheres with realistic dissipation and temperature,
475 part I: Mathematical development and propagation of waves into the thermosphere, Geophys.
476 Fluid Dyn., 1, 303-355, 1970.

477 Lindzen, R. S., and Kuo, H. L.: A reliable method for the numerical integration of a large class
478 of ordinary and partial differential equations, Mon. Wea. Rev., 97, 732-734, 1969.

Liu, A. Z., and Swenson, G. R.: A modeling study of O_2 and OH airglow perturbations induced by atmospheric gravity waves, J. Geophys. Res, 108, D4, 4151, doi:10.1029/2002JD002474, 2003.

Lopez-Gonzalez, M. J., et al.: Tidal variations of O_2 Atmospheric and OH(6-2) airglow and temperature at mid-latitude from SATI observations, Ann. Geophys., 23, 3579–3590, 2005.

Makhlouf, U. B., Picard, R. H., and Winick, J. R.: Photochemical-dynamical modeling of the measured response of airglow to gravity waves, 1: basic model for OH airglow, J. Geophys. Res., 100, 11,289–11,311, 1995.

Offermann, D., Friedrich, V., Ross, P., and Von Zahn, U.: Neutral gas composition measurements between 80 and 120 km, Planet Space Sci., 29, 747–764, 1981.

Oznovich, I., Walterscheid, R. L., Sivjee, G. G., and McEwen, D. J.: On Krassovsky's ratio for ter-diurnal hydroxyl oscillations in the winter polar mesopause, Planet Space Sci.,45(3), 385–394, 1997.

Oznovich, I., McEwen, D. J., and Sivjee, G. G.: Temperature and airglow brightness oscillations in the polar mesosphere and lower thermosphere, Planet Space Sci., 43, 1121–1130, 1995.

Sikha, P. R., Parihar, N., Ghodpage, R., and Mukherjee, G. K.: Characteristics of gravity waves in the upper mesosphere region observed by OH airglow imaging , Current Sciences, 98, No. 3, 392-397, 2010.

Reisin, E. R. and Scheer, J.: Gravity wave activity in the mesopause region from airglow measurements at El Leoncito, J. Atmos. Sol. Terr. Phys., 66, 655–661, 2004.

499 Reisin, E. R., and Scheer, J.: Characteristics of atmospheric waves in the tidal period range
500 derived from zenith observations of O_2(0-1) Atmospheric and OH (6-2) airglow at lower mid
501 latitudes, J. Geophys. Res., 101, 21,223–21,232, 1996.

502 Richmond, A. D.: Energy relations of atmospheric tides and their significance to approximate
503 methods of solution for tides with dissipative forces, J. Atmos. Sci., 32, 980-987, 1975.

504 Schubert, G., Hickey, M. P., and Walterscheid, R. L.: Heating of Jupiter's thermosphere by the
505 dissipation of upward propagating acoustic waves, Icarus, 163, 398-413, 2003.

506 Schubert, G., Walterscheid, R. L., and. Hickey, M. P.: Gravity wave-driven fluctuations in OH
507 nightglow from an extended, dissipative emission region, J. Geophys. Res., 96 (A8), 13,869–
508 13,880, 1991.

509 Takahashi, H., Buriti, R. A., Gobbi, D., and Batista, P. P.: Equatorial planetary wave signatures
510 observed in mesospheric airglow emissions, J. Atmos. Sol. Terr. Phys., 64, 1263–1272, 2002.

511 Takahashi, H., Sahai, Y., Batista, P. P., and Clemesha, B. R.: Atmospheric gravity wave effect
512 on the airglow O2(0-1) and OH (9-4) band intensity and temperature variations observed from
513 a low latitude station, Adv. Space Res.,12(10), 131–134, 1992.

514 Taylor, M. J., Gardner, L. C., and Pendleton, Jr. W. R.: Long-period wave signatures in
515 mesospheric OH Meinel (6,2) band intensity and rotational temperature at mid-latitudes, Adv.
516 Space Res., 27(6–7), 1171– 1179, 2001.

517 Taylor, M. J., Turnbull, D. N., and Lowe, R. P.: Coincident imaging and spectrometric
518 observations of zenith OH nightglow structure, Geophys. Res. Lett., 18, 1349–1352, 1991.

519 Taori, A., and Taylor, M. J.: Characteristics of wave induced oscillations in mesospheric O2
520 emission intensity and temperatures, Geophys. Res. Lett., 33, L01813,
521 doi:10.1029/2005GL024442, 2006.

522 Taori, A., Taylor, M. J., and Franke, S.: Terdiurnal wave signatures in the upper mesospheric
523 temperature and their association with the wind fields at low latitudes (20◦N), J. Geophys.
524 Res., 110, D09S06, doi: 10.1029/2004JD004564, 2005.

525 Taori, A., Jayaraman, A., Kamalakar, V.: Imaging of mesosphere–thermosphere airglow
526 emissions over Gadanki (13.51N, 79.21E)-first results, J. Atmos. Sol. Terr. Phys. 93, 21–28,
527 http://dx.doi.org/10.1016/j.jastp.2012.11.007, 2013.

528 Tarasick, D. W., and Shepherd, G. G.: Effects of gravity waves on complex airglow chemistries:
529 1. $O_2(b^1\sum^+_g)$ emission, J. Geophys. Res., 97, 3185–3193, 1992a.

530 Tarasick, D. W., and Shepherd, G. G.: Effects of gravity waves on complex airglow chemistries:
531 2. OH emission, J. Geophys. Res., 97, 3195–3208, 1992b.

532 Vargas, F., Swenson, G., Liu, A., and Gobbi, D.: $O(^1S)$, OH, and $O_2(b)$ airglow layer
533 perturbations due to AGWs and their implied effects on the atmosphere, J. Geophys. Res, 112,
534 D14102, doi:10.1029/2006JD007642, 2007.

535 Viereck, R. A., and Deehr, C. S.: On the interaction between gravity waves and the OH Meinel
536 (6-2) and O2Atmospheric (0-1) bands in the polar night airglow, J. Geophys. Res., 94, 5397–
537 5404, 1989.

538 Walterscheid, R. L., and Schubert, G.: Dynamical-chemical model of fluctuations in the OH
539 airglow driven by migrating tides, stationary tides, and planetary waves, J. Geophys. Res.,
540 100, 17,443–17,449, 1995.

541 Walterscheid, R. L., and Hickey, M. P.: One-gas models with height-dependent mean molecular
542 weight: Effects on gravity wave propagation, J. Geophys. Res., 106, 28,831-28,839, 2001.

543 Walterscheid, R. L., Schubert, G., and Hickey, M. P.: A Comparison of Theories for Gravity
544 Wave Induced Fluctuations in Airglow Emissions, J. Geophys. Res., 99, 3935, 1994.

545 Walterscheid, R. L., Schubert, G., and Hickey, M. P.: Comparison of theories for gravity wave
546 fluctuations in airglow emissions, J. Geophys. Res., 99, 3935–3944, 1994.

547 Walterscheid, R. L., Schubert, G., and Straus, J. M.: A dynamical chemical model of wave-
548 driven fluctuations in the OH nightglow, J. Geophys. Res., 92, 1241 – 1254, 1987.

549

550 **Figure captions:**

551 **Figure 1.** Nocturnal variability in the mesospheric OH emissions on 26-27 January 2011. The
552 upper panels represent the mean deviations in (a) temperature and (b) intensity data. Bottom
553 panels represent (c) temperature and (d) intensity residuals. Solid line curves in each plot show
554 the result of simple best-fit cosine model which estimates the dominant wave periodicity,
555 amplitude and phase of waves in the data obtained over Kolhapur.

556

557 **Figure 2 (a)** A comparison of Krassovsky parameters of data to their respective wave periods.
558 The x -axis shows the wave periodicity and the y-axis is for Krassovsky parameters (η and Φ) in
559 each plot. A close resemblance between the observational values and discrepancy between the

observational and theoretical estimates are notable. The legends in the figure are as following: ((η : 1 (for 2010 year), 2 (for 2011 year), present study ; 3,Schubert et al. 500 km; 4, Schubert et al. 1000 km; 5, Tarasick and Shepherd 500 km; 6,Tarasick and Shepherd 1000 km; 7, Takahashi et al. (1992); 8, Oznovich et al. (1995); 9, Drob et al. (1996); 10, Reisin and Scheer (1996); 11, Taylor et al. (2001); 12,Guhary et al (2008); 13, Walterscheid and Schubert (1995); 14, Lopez-Gonzalez et al. (2005); 15, Oznovich et al. (1997)); 16, Viereck and Deehr (1989).

Figure 2 (b) A comparison of phi values to their respective wave periods (Φ: 1, 2, present study; 3,Schubert et al. 500 km; 4, Schubert et al. 1000 km; 5, Tarasick and Shepherd 500 km; 6, Tarasick and Shepherd 1000 km; 7,Viereck and Deehr (1989); 8, Oznovich et al. (1995); 9, Drob et al. (1996); 10, Reisin and Scheer (1996); 11, Taylor et al. (2001); 12, Walterscheid and Schubert (1995); 13, Guhary et al.(2008); 14, Lopez-Gonzalez et al. (2005); 15, Oznovich et al. (1997)).

Figure 2c. Deduced vertical wavelength (VW) for both the short and long period wave as function of wave periodicity. Also shown comparison with values obtained by other investigators.

Figure 3a. Shown comparison with η calculated by observation of both year and Full wave model simulation with their respective wave period. Pink and olive lower half filled square shows the 2010 and 2011 year η observations.

Figure 3b. Phase values for both the short and long period wave as function of wave periodicity comparison with values obtained full wave model simulation.

Figure 3c. Deduced vertical wavelength (VW) for both the short and long period wave as function of wave periodicity comparison with values obtained full wave model simulation (VW :

583 1,FWM simulation of VW for 50 m/s horizontal phase velocity; 2, FWM simulation of VW for
584 100 m/s horizontal phase velocity; 3, FWM simulation of VW for 150 m/s horizontal phase
585 velociy; 4 and 5 present study (for 2010 and 2011 year)).
586 **Figure 4**. The monthly (February, March and April) mean values of OH emission rates are
587 shown in plot. The straight lines plot the data for the year 2010 while the dashed lines represent
588 the year 2011.
589
590 **Table 1.** Comparisons of deduced wave parameters in 2010,2011 years with MEI index and OH
591 altitudes. The observed quantities are mean for their representative wave periods. (JFM-January,
592 February and March months like this)
593

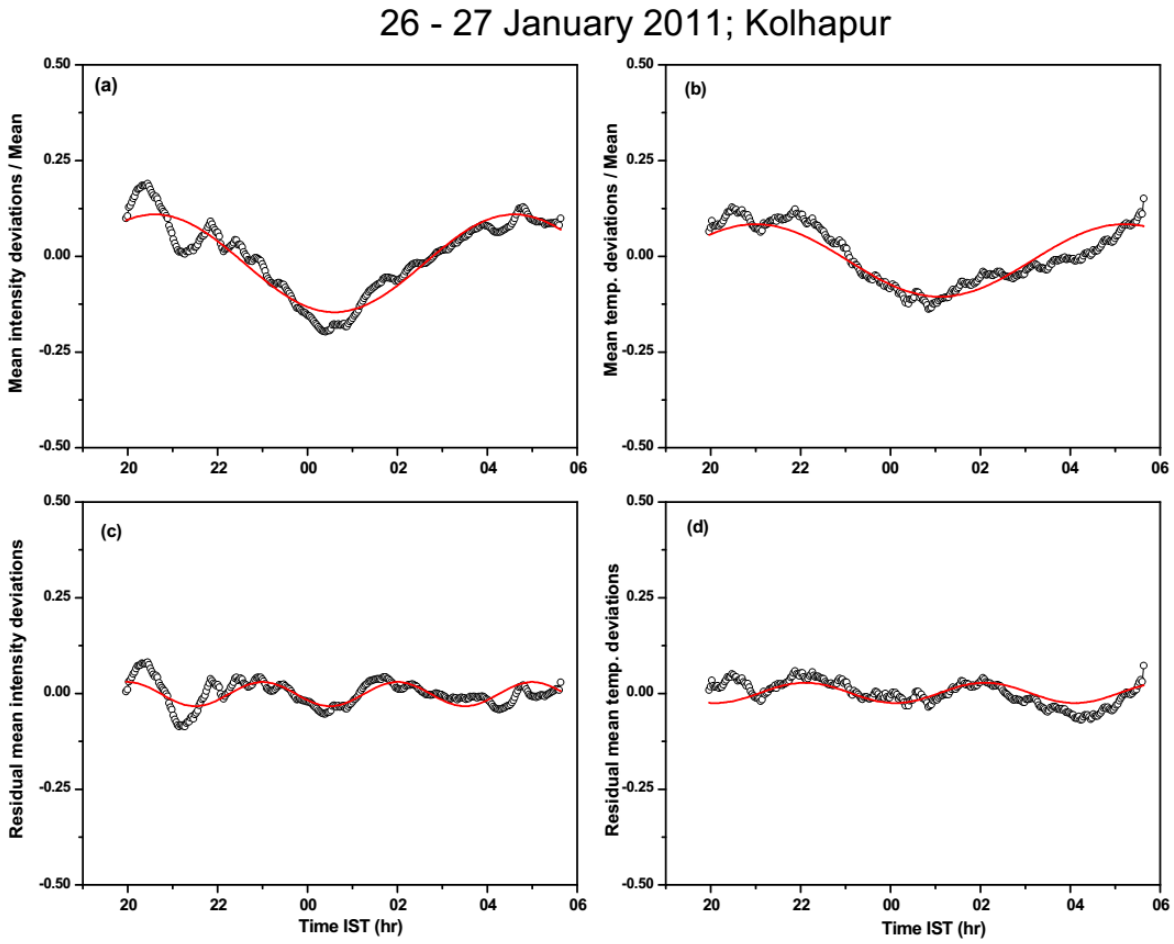
26 - 27 January 2011; Kolhapur
(a)
(b)
(c)
(d)
Mean intensity deviations / Mean
Mean temp. deviations / Mean
Residual mean intensity deviations
Residual mean temp. deviations
Time IST (hr)
Time IST (hr)
0.50
0.25
0.00
-0.25
-0.50
20
22
00
02
04
06

Figure 1.

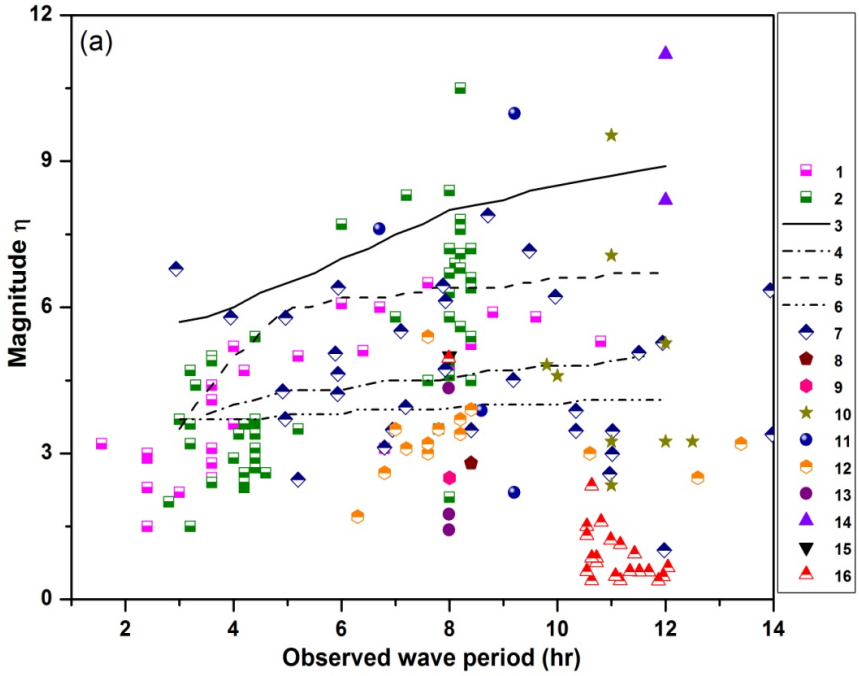

597

598 Figure 2(a)

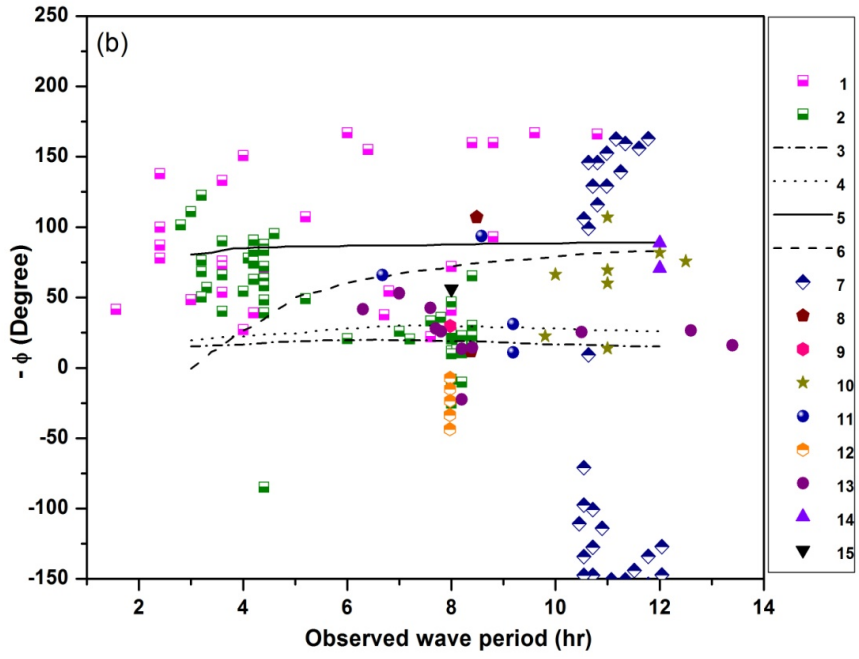

599

600 Figure 2(b)

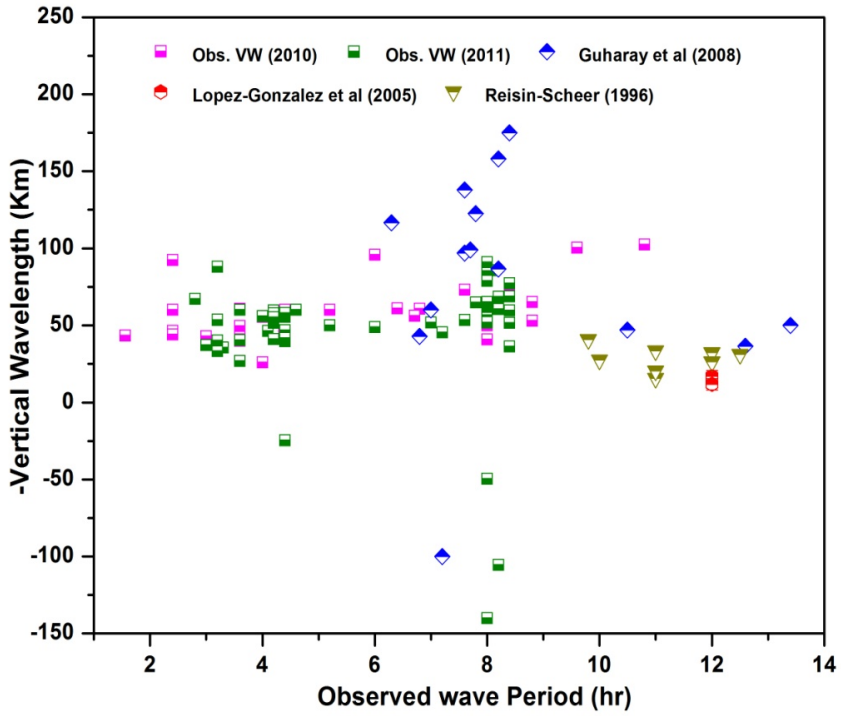

601

602 Figure 2(c)

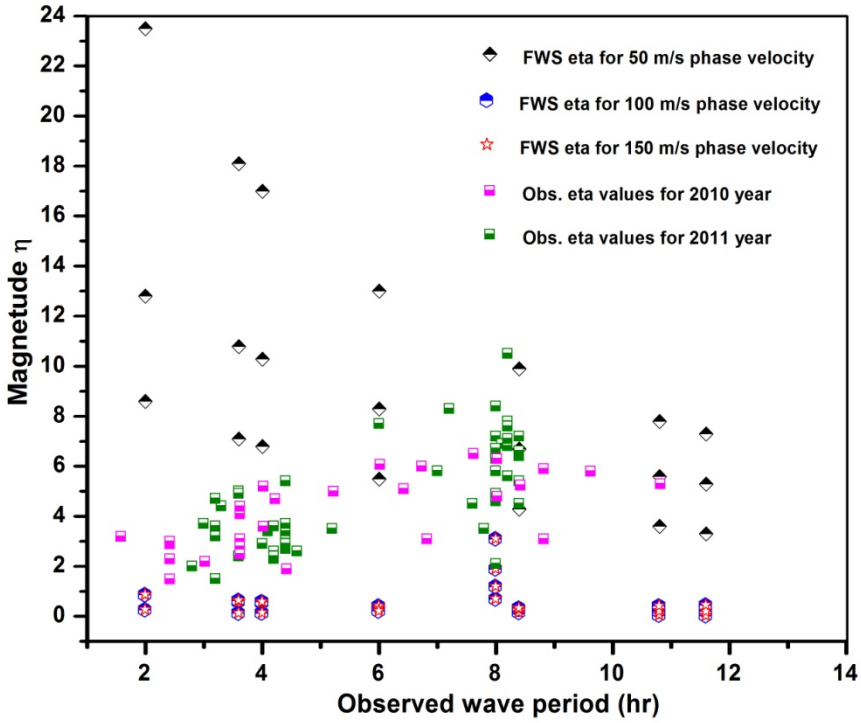

603

604 Figure (3a)

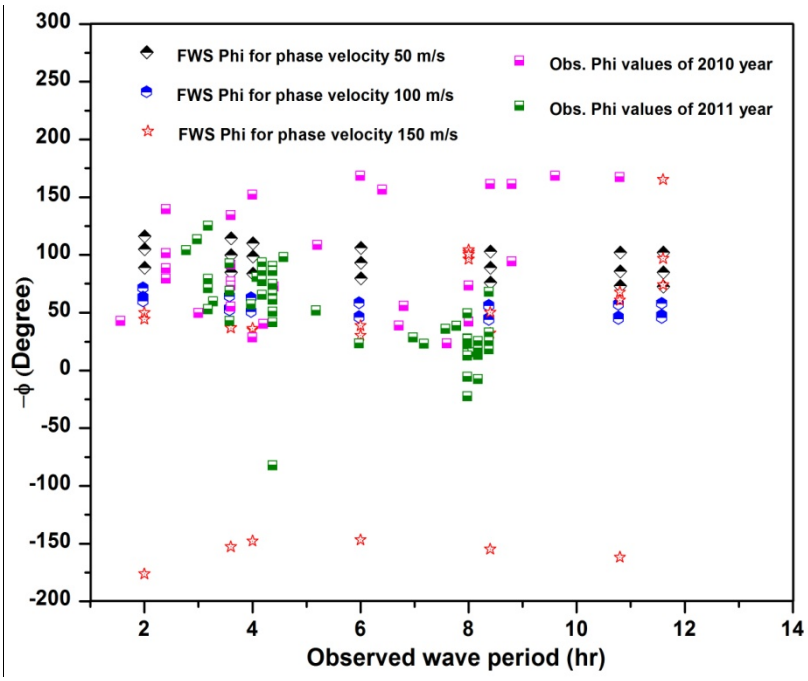

605

606 Figure 3(b)

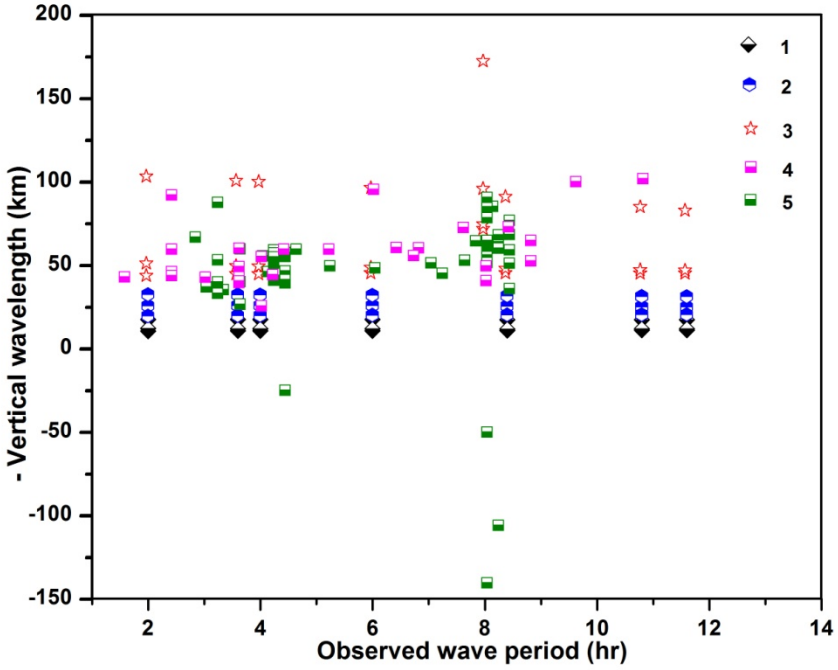

607

608 Figure 3 (c)

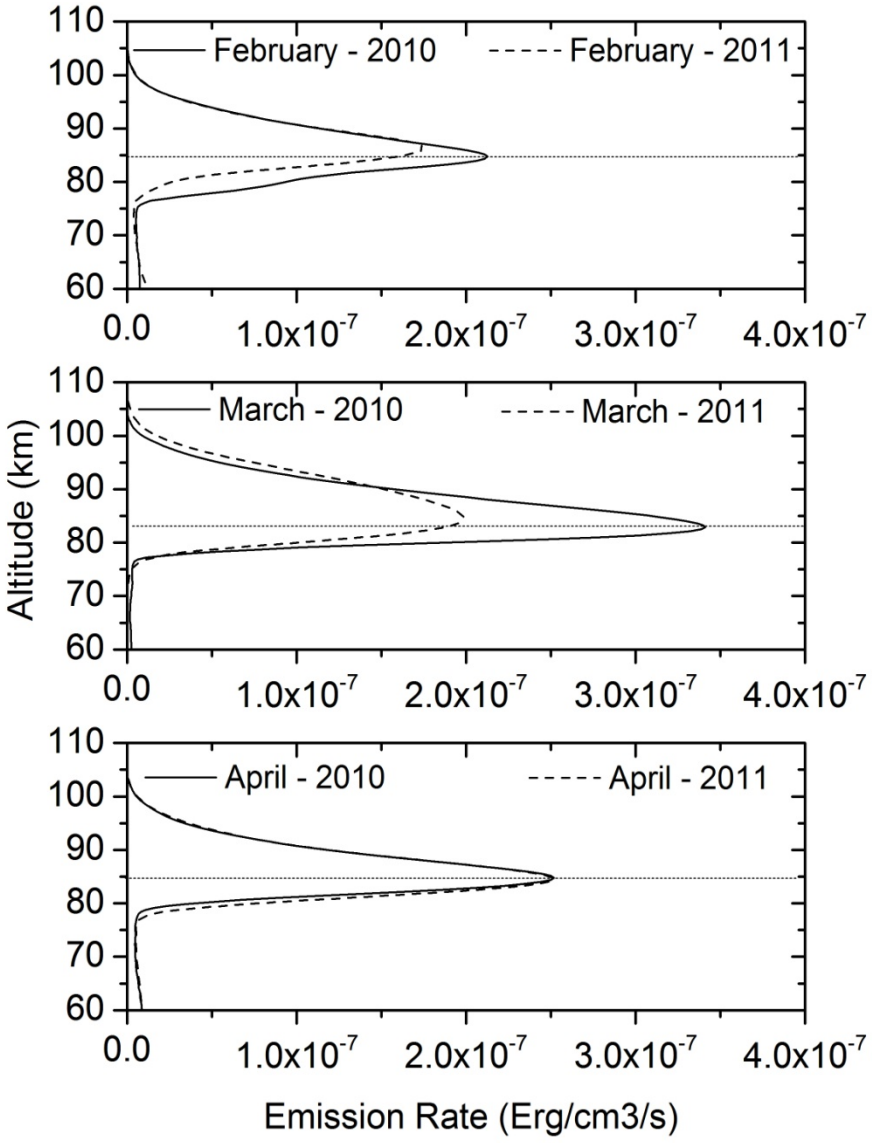

609

610 Figure 4.

611

612

613

614

615

616 Table 1.

Year	**Mean η** (± Errors)		**Mean (-Φ) (Deg.)**		**Mean (-VW) (km)**		**OH altitude (km)**	**MEI index**				
	Long wave period	Short wave period	Long wave period	Short wave period	Long wave period	Short wave period		JFM	FMA	MAM	SON	OND
2010	4.4 ± 1	2.3 ±0.9	90.6±40	70.4± 45	60.2 ± 20	42.8 ± 15	82 km to 85.1 km during February – April	1.1	0.8	0.5	-1.4	-1.3
2011	5.7 ± 1.7	2.7 ±0.6	33.8±40	64.4± 40	77.6 ± 40	59.2 ± 30	85.1 km to 86 km during February – April	-1.1	-0.8	-0.6	-0.9	-0.9

617

618